



HAL
open science

Improvement of the Electrochemical Performance of $\text{Ln}_{0.58}\text{Sr}_{0.4}\text{Fe}_{0.8}\text{Co}_{0.2}\text{O}_{3-\delta}$ IT-SOFC Cathodes by Ternary Lanthanide Combinations (La-Pr-Sm)

Vicente B Vert, Jose M. Serra

► **To cite this version:**

Vicente B Vert, Jose M. Serra. Improvement of the Electrochemical Performance of $\text{Ln}_{0.58}\text{Sr}_{0.4}\text{Fe}_{0.8}\text{Co}_{0.2}\text{O}_{3-\delta}$ IT-SOFC Cathodes by Ternary Lanthanide Combinations (La-Pr-Sm). Fuel Cells, 2010, 10 (4), pp.693. 10.1002/fuce.200900166 . hal-00552365

HAL Id: hal-00552365

<https://hal.science/hal-00552365>

Submitted on 6 Jan 2011

HAL is a multi-disciplinary open access archive for the deposit and dissemination of scientific research documents, whether they are published or not. The documents may come from teaching and research institutions in France or abroad, or from public or private research centers.

L'archive ouverte pluridisciplinaire **HAL**, est destinée au dépôt et à la diffusion de documents scientifiques de niveau recherche, publiés ou non, émanant des établissements d'enseignement et de recherche français ou étrangers, des laboratoires publics ou privés.



**Improvement of the Electrochemical Performance of
Ln_{0.58}Sr_{0.4}Fe_{0.8}Co_{0.2}O_{3-δ} IT-SOFC Cathodes by Ternary
Lanthanide Combinations (La-Pr-Sm)**

Journal:	<i>Fuel Cells</i>
Manuscript ID:	face.200900166.R1
Wiley - Manuscript type:	Original Research Paper
Date Submitted by the Author:	30-Dec-2009
Complete List of Authors:	Vert, Vicente; Instituto de Tecnologia Quimica (UPV-CSIC) Serra, Jose; Instituto de Tecnologia Quimica (UPV-CSIC)
Keywords:	SOFC, Cathode, lanthanide, perovskite, cobaltite, ferrite



Improvement of the Electrochemical Performance of $\text{Ln}_{0.58}\text{Sr}_{0.4}\text{Fe}_{0.8}\text{Co}_{0.2}\text{O}_{3-\delta}$ IT-SOFC Cathodes by Ternary Lanthanide Combinations (La-Pr-Sm)

Vicente B. Vert¹, José M. Serra^{1,*}

¹Instituto de Tecnología Química (UPV-CSIC), Av. Los Naranjos s/n, E-46022, Valencia, Spain

[*] Corresponding author, jsalfaro@itq.upv.es; Fax: +34.963.877.809

Abstract

Active perovskite-based SOFC cathodes have been developed through lanthanide combination in the $(\text{La}_{1-x-y}\text{Pr}_x\text{Sm}_y)_{0.58}\text{Sr}_{0.4}\text{Fe}_{0.8}\text{Co}_{0.2}\text{O}_{3-\delta}$ system following a ternary mixture experimental design. These compositions were prepared through a sol-gel method and characterized by electrochemical impedance spectroscopy (EIS) as symmetrical cells on GDC-electrolyte samples in the 450-650 °C temperature range. The electrochemical properties of the single lanthanide-based $\text{Ln}_{0.58}\text{Sr}_{0.4}\text{Fe}_{0.8}\text{Co}_{0.2}\text{O}_{3-\delta}$ compounds were enhanced when different lanthanides were combined together in the same crystalline structure. The observed improvement **does** not follow a mere additional effect of the performance from the parent $\text{Ln}_{0.58}\text{Sr}_{0.4}\text{Fe}_{0.8}\text{Co}_{0.2}\text{O}_{3-\delta}$ compounds, i.e. it **does** not follow a linear behaviour, and the better performance is ascribed to synergetic catalytic effects among lanthanide cations. A reduction in electrode polarization resistance with respect to non-substituted compositions is stated for most $\text{Ln}_{0.58}\text{Sr}_{0.4}\text{Fe}_{0.8}\text{Co}_{0.2}\text{O}_{3-\delta}$ electrode compositions combining two or three lanthanides. Samarium addition to the electrode material involves a substantial reduction in the activation energy and the reduction degree is directly dependant on the samarium amount incorporated in the lattice. The best performing composition comprises a praseodymium-rich lanthanum-based electrode material. The experimental data derived from the ternary mixture design were modelled using non-linear functions and this modelling allowed finding an electrode composition minimizing the polarization resistance while maintaining the activation energy at reduced values. Selected cathode compositions were tested in fully-assembled anode-supported cells and electrochemical characterization supports the cooperative effect of lanthanide combination.

Keywords: Cathode, Perovskite, IT-SOFC, Ferrite, Cobaltite, Oxygen Conductor, Lanthanide, Mixture Design

1 Introduction

Solid oxide fuel cells (SOFCs) are becoming promising candidates for highly efficient energy generation from conventional and biomass-derived fuels due to different reasons: (i) electricity can be obtained directly from a fuel; (ii) the sub-product is a high quality hot gas stream, usable in (micro)turbines and for building central heating (CHP units [1]); (iii) zero-emission operation is achieved when hydrogen is fuelled; (iv) SOFCs can operate besides H_2 with light hydrocarbons, methanol or even bio-alcohols without extensive fuel purification and reforming; and (v) SOFCs are noiseless and modular. However, conventional SOFCs need to operate in the 800-1000

1
2
3 °C temperature range. The reduction of the operating temperature below 700 °C implies
4 that the electrode polarization resistance of classical cathodes [2, 3, 4] limits the whole
5 cell operation, and consequently the performance is significantly lessened. Therefore,
6 there exists the need of developing new cathode materials with sufficient chemical
7 stability and electrochemical activity to enable the operation at lower temperatures with
8 acceptable power density.
9

10
11 From the cathode materials being developed for operation at intermediate
12 temperature, lanthanide ferrites and/or cobaltites are the most outstanding materials.
13 High performing electrodes based on this family comprise systems like
14 $\text{La}_{0.6}\text{Sr}_{0.4}\text{Co}_{0.2}\text{Fe}_{0.8}\text{O}_{3-\delta}$ (LSFC) [5, 6, 7], $\text{Sm}_{0.5}\text{Sr}_{0.5}\text{CoO}_{3-\delta}$ (SSC) [8], $\text{Gd}_{1-x}\text{Sr}_x\text{CoO}_{3-\delta}$
15 [9] or $\text{Pr}_{0.8}\text{Sr}_{0.2}\text{FeO}_{3-\delta}$ (PSF) [10, 11]. Lanthanides have a positive effect in the
16 electrochemical activity for oxygen reduction due to their redox couples (like $\text{Pr}^{+3} \leftrightarrow \text{Pr}^{+4}$
17 or $\text{Sm}^{+3} \leftrightarrow \text{Sm}^{+2}$) and their controlled basicity. Different studies have shown the effect of
18 the lanthanide nature in $\text{Ln}_{1-x}\text{Sr}_x\text{Co}_{0.2}\text{Fe}_{0.8}\text{O}_{3-\delta}$ -like electrodes [12, 13, 14] as IT-SOFC
19 cathodes. However, these studies have been conducted in terms of the electrochemical
20 performance when just one lanthanide is partially-substituting the basic strontium
21 ferrite-cobaltite structure. Among the different lanthanides, it was found that La, Sm
22 and Pr [12] show the highest potential for further material development due to their
23 complementary properties for the oxygen reduction reaction at intermediate
24 temperatures. In addition, higher stability of such materials in comparison with other
25 studied IT-SOFC cathodes, as $\text{Ba}_{0.5}\text{Sr}_{0.5}\text{Co}_{0.8}\text{Fe}_{0.2}\text{O}_{3-\delta}$ [15], makes them more suitable
26 for standard operation conditions.
27
28
29
30

31
32 In the present work, the possible cooperative effects arising from the combination of
33 various lanthanides on the same strontium ferrite-cobaltite perovskite structure have
34 been thoroughly investigated. Specifically, a series of perovskite compounds based on
35 La, Pr and Sm and their combinations in a $(\text{La}_{1-x-y}\text{Pr}_x\text{Sm}_y)_{0.58}\text{Sr}_{0.4}\text{Fe}_{0.8}\text{Co}_{0.2}\text{O}_{3-\delta}$
36 compound were prepared following a ternary mixture experimental design and
37 characterized in terms of oxygen activation and transport by electrochemical impedance
38 spectroscopy analysis on symmetrical cells as a function of temperature (450-650 °C)
39 and oxygen partial pressure (0.2, 0.1, 0.02 atm). Finally, selected cathode compositions
40 were deposited on anode (Ni-8YSZ)-supported cells and electrochemically tested using
41 humidified hydrogen as fuel.
42
43

44 2 Experimental

45 Perovskite powders were synthesized through a complexation-polymerization
46 method [16] by mixing appropriate metal nitrates with citric acid in an aqueous
47 solution, followed by an ethylene-glycol polymerization through gradual heat treatment
48 at increasing temperatures up to 160 °C. After foaming and drying, a calcination step at
49 1000 °C was necessary to obtain the perovskite compounds with sufficient crystallinity,
50 as confirmed by X-ray diffraction analysis. XRD was carried out using monochromated
51 CuK_α radiation on a PANalytical X'Pert Pro equipment.
52
53
54

55 The as-calcined powders were milled with 3YSZ balls (Tosoh) in acetone for 15 h
56 for ensuring proper particle size distribution. Screen-printable inks were fabricated by
57 mixing the milled powders with a solution of ethylcellulose in terpineol (6% wt.) and
58 refined using a three roller mill (Exakt). Those inks were applied on both sides of dense
59 ~1 mm-thick 20% mol-gadolinium doped ceria (GDC) disks and finally calcined in air
60 at 1060 °C for 2 h. Dense GDC disks were fabricated by uniaxial pressing of powder

(Treibacher, Austria), with an averaged grain size of 0.2 μm , at ~ 120 MPa and final sintering at 1300 $^{\circ}\text{C}$ for 2 h.

Two-point configuration symmetrical cells were tested by electrochemical AC impedance spectroscopy (EIS) using a 0 V DC – 50 mV AC signal in a 0.01 - $3 \cdot 10^5$ Hz frequency range in a Solartron 1470E+1455A FRA module equipment, measured in the range from 450-650 $^{\circ}\text{C}$ and for different oxygen partial pressure atmospheres (100%, 50% and 10% Air, i.e., 0.21, 0.105 and 0.021 atm of oxygen) by means of diluting the air flow with argon but maintaining a total constant flow of 100 $\text{mL} \cdot \text{min}^{-1}$. Cells were measured at decreasing temperatures in intervals of 50 $^{\circ}\text{C}$, starting at 650 $^{\circ}\text{C}$.

Reproducibility was assessed for several samples and the error obtained for the polarization resistance was $\pm 5\%$.

Voltamperometric measurements have been carried out on fully assembled SOFC using FZJ-standard half cells [4]. Disk-shaped anode-supported cells with diameter 15.5 mm consisted of an anode substrate (averaged thickness of 1500 μm), an anode functional layer (thickness in the range 5–10 μm), and an 8YSZ electrolyte (thickness in the range 5–10 μm). The anode functional layer (NiO/8YSZ) and the electrolyte (8YSZ, Tosoh, Japan) were produced by vacuum slip casting and co-fired at 1400 $^{\circ}\text{C}$, resulting in a gastight 8 μm -thick electrolyte. On top of this electrolyte layer, a $\text{Ce}_{0.8}\text{Gd}_{0.2}\text{O}_{1.9}$ (GDC) layer (Treibacher), acting as a cation-diffusion barrier, was applied by screen printing (final thickness: 5 μm) and sintered at 1250 $^{\circ}\text{C}$ [7, 17]. On top of the GDC protective layer a ~ 40 μm cathode layer was applied by screen-printing. Electrochemical single cell testing was done at 600 and 650 $^{\circ}\text{C}$ using humidified hydrogen (150 $\text{mL} \cdot \text{min}^{-1}$) as fuel at the anode side and air (150 $\text{mL} \cdot \text{min}^{-1}$) at the cathode side. Sealing was achieved using gold gaskets. After electrochemical analysis, fracture cross-sections of graphite sputtered cells were analyzed by SEM using a JEOL JSM6300 electron microscope.

3 Results and discussion

3.1 Structural Characterization

The materials synthesized combining multiple lanthanides following the $(\text{La}_{1-x-y}\text{Pr}_x\text{Sm}_y)_{0.58}\text{Sr}_{0.4}\text{Fe}_{0.8}\text{Co}_{0.2}\text{O}_3$ formula are listed in Table 1. Since the total amount of the three elements (La, Pr and Sm) is constant, the different perovskite compositions can be arranged in a ternary mixture diagram (Figure 1). Indeed, single, binary and ternary lanthanide combinations are systematically distributed in the ternary diagram of Figure 1. Room temperature X-ray diffraction patterns displayed in Figure 2 show that all electrode compositions could be obtained as pure perovskite phase and only minor impurities of Fe-Co spinel are observed in the compounds La1SFC and La0.5Pr5SFC (plus symbol) and in smaller ratio in the La0.5Sm0.5SFC composition. Moreover, it can be observed that some electrode compositions exhibit different degrees of distortion of the perovskite symmetry ascribed to the orthorhombic crystal ordination [18]. The diffraction peaks assigned to the orthorhombic phase are highlighted in Figure 2 (solid circles). This orthorhombic phase becomes more significant in compositions with high amounts of samarium in single (Sm1SFC, Figure 2-e) or in praseodymium-combined perovskites [19] like Pr0.5Sm0.5SFC (Figure 2-f) and La0.17Pr0.17Sm0.66SFC (Figure 2-j) compounds. The occurrence of the orthorhombic distorted phase is ascribed to the reduction of the averaged ionic radius of the A-site cations through the introduction of relatively smaller cations (with respect to La^{+3} 1.36 \AA) as Sm^{+3} with a radius of 1.24 \AA

in 12-fold coordination [20, 21]. **La_{0.5}Sm_{0.5}SFC perovskite have no significant occurrence of orthorhombic symmetry due to the presence of the bigger La⁺³ cation.**

From the X-ray diffraction patterns, lattice parameters were computed [22] for the perovskite compounds and a pseudo-cubic parameter [23, 24] a' (cube root of lattice volume) was obtained using the lattice parameters of the predominant perovskite phase. **This a' lattice parameter is an approximation of lattice size and can be used for comparing the cell size variation as a function of the lanthanide mixture.** From Figure 3, a trend in the lattice size evolution can be observed when replacing the lanthanide by another cation with lower ionic radius [20], being in agreement with the lanthanide contraction [25]. Accordingly, the gradual introduction of lanthanide cations with decreasing radius leads to decreasing perovskite dimensions, following a rather linear behaviour. Indeed, the trends in unit cell size variation obtained for non-substituted (single) Ln1SFC compositions are followed when combining lanthanides in binary and ternary compositions. For instance, the La_{0.33}Pr_{0.33}Sm_{0.33}SFC compound has an averaged lattice size in between the three single Ln1SFC compositions, as expected from a linear behaviour. In fact, this linear trend becomes more evident comparing the **averaged** filled bars in Figure 3, which represent the proportion of the different lanthanides in **each** compound. Nonetheless, such lattice size differences are not very significant as it can be concluded from the ordinate axis (a') scale in Figure 3. The cell parameters range from **3.841 to 3.876 Å**.

The slight variation in electrode microstructure of the single lanthanide Ln1SFC compositions [26] becomes diminished when these lanthanides are combined together in the same perovskite structure, as stated from the SEM pictures in Figure 4. Different ternary and binary lanthanide substituted electrodes are compared in Figure 4 by SEM and no significant microstructural differences can be found, i. e., neither the particle size nor the porosity of electrodes sintered at 1060 °C are drastically modified through the compositional variation of the perovskite lattice.

3.2 EIS Characterization Results

Oxygen activation is the basis of the processes occurring in a porous SOFC cathode (or in the porous electrode of symmetrical cells) involving [27, 28, 29, 30, 31]: oxygen diffusion through porous cathodes, adsorption of molecular oxygen on the cathode catalyst surface, reduction of molecular oxygen into different oxygen ionic species on cathode surface entailing electron transfer, oxygen ion incorporation into the bulk, transport of oxygen ion or molecular adsorbed oxygen from the cathode surface to the electrolyte interface and transfer from the interface to the electrolyte bulk. EIS experimental data **were** recorded for each material and temperature and the polarization contributions were modelled as two arcs in the negative imaginary part of Nyquist (Cole-Cole) plot (see [32] and Supplementary Material for more detailed explanation). These two arcs can be more or less overlapped depending on the characteristics of each electrode composition. The high frequency arc is ascribed to the transfer of active oxygen species (vacancies/ions or adsorbed atoms) to the electrolyte surface [33]; that motion of species is associated or characterized by a resistance (R_T) and an electrochemical capacitance (C_T). However, for compensating the non-homogeneity of electrodes, the best fitting is achieved by using a constant phase element (Q_T) instead of a pure capacitor, since the high frequency arc appears depressed for all measured symmetrical cells. On the other hand, the low frequency arc is related to the solid state

diffusion coupled to a *chemical reaction* occurring on the electrode surface [34], when bulk and surface diffusion are in competition. This behaviour has been described by Adler [34], and can be modelled by a Gerischer element [35] since it is mathematically isomorphic. Raw impedance data present a deviation from the origin of the Nyquist plot that corresponds to the ohmic contribution of the electrolyte [36] and an inductive tail at high frequencies due to platinum leads.

Figure 5 shows the Arrhenius plot of the electrode polarization resistance (R_p) at different temperatures of the whole ternary mixture design. The data are displayed in three different electrode groups, i.e., single, binary and ternary compounds. Polarization resistance values obtained for the binary and ternary combinations of lanthanides are significantly lower than those for the best single electrode La1SFC. Nevertheless, La_{0.17}Pr_{0.17}Sm_{0.66}SFC electrode shows a lower oxygen activation performance and it performs worse than the single Sm1SFC composition. This behaviour is ascribed to the fact that in this composition the ratio of orthorhombic symmetry is higher than for the rest of samarium-based compositions as explained previously (Figure 2).

In the studied temperature range (see Figure 5), the electrode composition La_{0.5}Pr_{0.5}SFC has the lowest electrode polarization resistance. Interestingly, when decreasing the temperature the compound containing equivalent amounts of lanthanum and samarium (La_{0.5}Sm_{0.5}SFC) achieves R_p values as low as the previous compositions. Another interesting ternary composition is the one containing more praseodymium (La_{0.17}Pr_{0.66}Sm_{0.17}SFC) and it behaves in between La-Pr and La-Sm compositions abovementioned. Summing up, most of the binary and ternary lanthanide combinations led to a reduction of the R_p values when compared with parent single-lanthanide compounds, although only the three aforementioned combinations resulted in a very substantial improvement of the electrochemical performance for oxygen activation. Additionally, in each electrode group displayed in Figure 5 there is a composition that reduces the polarization resistance when decreasing the temperature compared to the others in the plot. In Figure 5a (single compounds), the composition Sm1SFC evolves towards lower polarization resistances with decreasing temperatures with respect to the La or Pr-based electrodes. In Figure 5b (binary compounds), the equivalent evolving composition is La_{0.5}Sm_{0.5}SFC while, in Figure 5c (ternary compounds), the La_{0.33}Pr_{0.33}Sm_{0.33}SFC electrode achieves relatively low R_p at the lowest temperatures.

The previous electrode compositions have different amounts of samarium in the position. The significant reduction of electrode polarization resistance observed for these compositions at the lowest measured temperatures can be explained in terms of activation energy. The apparent activation energy is depicted by the bars in Figure 6 whilst the relative amount of samarium is described by the squared line on the bars (samarium percentage must be read in the inverse scale of the right-handed axis). Compositions with lower activation energy values (bars) are those with higher degrees of samarium substitution (squared line). Single Sm1SFC (100% Sm content) has the lowest activation energy and the compositions with more than 33% Sm substitution have closer activation energy values. On the other hand, compositions with 33% or lower samarium content have higher activation energy values. Electrodes with low activation energy values are desired for low temperature applications although the electrode R_p should be low in the whole temperature range. Consequently, compositions containing enough samarium will be of particular interest (like

La_{0.5}Sm_{0.5}SFC) for very low temperature applications. Albeit La_{0.17}Pr_{0.17}Sm_{0.66}SFC composition has the highest samarium content and indeed the lowest activation energy value of the n-ary compositions, its performance as electrode does not fulfil the desired operating conditions (see polarization resistance values in Figure 5c) and this might be caused by the formation of a less conductive orthorhombic structure [37, 38].

In addition, when samarium or praseodymium are incorporated into the perovskite lattice structure, the oxygen reaction rate constant k is increased as extracted from equivalent circuit model (see Supplementary Material for details). From the analyzed compounds, all n-ary compositions containing samarium and/or praseodymium have high oxygen reaction rate values, probably due to the catalytic redox couple of samarium ($\text{Sm}^{+3}/\text{Sm}^{+2}$) and praseodymium ($\text{Pr}^{+4}/\text{Pr}^{+3}$), which would promote the oxygen reduction steps into different $\text{O}_2^{\delta-} / \text{O}^{\delta-}$ surface species and the subsequent incorporation into the perovskite bulk. Moreover, the presence of Sm^{+2} cations will lead to (i) the formation of more oxygen vacancies and (ii) the variation of the oxidation state of the catalytic B-site cations [24] ($\text{Co}^{+2} \rightarrow \text{Co}^{+3} \rightarrow \text{Co}^{+4}$, $\text{Fe}^{+2} \rightarrow \text{Fe}^{+3} \rightarrow \text{Fe}^{+4}$). These changes in the lattice oxidation states would lead to higher surface exchanges. Nevertheless, the samarium-enriched La_{0.17}Pr_{0.17}Sm_{0.66}SFC composition does not present such a high exchange rate constant and this might be linked again to the significant presence in the electrode of less conductive orthorhombic symmetry phase with respect to the major cubic symmetry phase.

Two of the compounds showing the highest reaction rate constant are La_{0.5}Sm_{0.5}SFC and La_{0.5}Pr_{0.5}SFC and these electrode compositions exhibited low polarization resistances (Figure 5) whereas the electrode Pr1SFC has one of the lowest k values and high polarization resistance. This fact evidences that the surface reaction is one limiting step in the cathode performance and the careful “design” of the catalytic surface will contribute markedly to the overall cathode improvement. Figure 7 supports this effect, in where the electrode polarization resistance (R_p) and the reaction rate constant (k) are plotted for three selected electrode compositions (Pr1SFC, La_{0.5}Sm_{0.5}SFC and La_{0.5}Pr_{0.5}SFC) as a function of temperature. High reaction rate constants are related to low polarization resistances. Nevertheless, this variation does not follow a linear evolution. The addition of samarium slightly increases the k value when compared to the same praseodymium addition, as concluded for the comparison between La_{0.5}Pr_{0.5}SFC and La_{0.5}Sm_{0.5}SFC in the bottom of Figure 7. However, it is not a direct evidence that La_{0.5}Sm_{0.5}SFC composition has lower polarization resistance than La_{0.5}Pr_{0.5}SFC. It should be considered that the cathode performance is affected additionally by other parameters simultaneously varied in the composition screening, i.e., changes in the material (electronic and ionic) conductivity, bonding to the electrolyte, porosity, etc. In Figure 7, it is also shown the effect of the oxygen partial pressure on R_p and k . The rate constant clearly diminishes with decreasing oxygen partial pressures and this oxygen sensibility is dependant on the electrode formulation, i.e., La_{0.5}Pr_{0.5}SFC, La_{0.5}Sm_{0.5}SFC compounds are more affected by air dilution than Pr1SFC. On the other hand, electrode polarization is slightly affected by the air dilution and only at high temperatures it is more sensible to the air dilution. The mismatch between the quantitative effects of the oxygen partial pressure on k and R_p could indicate that oxygen surface reduction and incorporation to the crystallite is certainly reduced with decreasing oxygen partial pressures whereas the oxygen-ion transport is still maintained due to the significant contribution of surface diffusion mechanism [39].

3.3 Modelling of the Ternary Mixture Space

As aforementioned, all synthesized compositions can be arranged in a ternary mixture diagram (Figure 1). Firstly, the a' cell parameter was fitted to a linear regression model, in which the independent variables are the content of each lanthanide (Sm, Pr and La) and the dependent variable is the lattice parameter. The linear regression could predict most of the compounds although some slight deviation from the linear behaviour could be stated. Using a simple artificial neural network model it was possible to obtain a non-linear model able to predict the whole experimental data. A simulation of the a' lattice parameter using this model is displayed in the ternary diagram arrangement in Figure 8a. The slight deviation of the linearity is attributed mainly to two aspects: (1) the presence of the orthorhombic symmetry for different Sm-containing compounds; and (2) the changes in the oxidation state of Fe, Co, Pr and Sm, and the subsequent changes in the oxygen stoichiometry, i.e., oxygen vacancy concentration. As a result, this structural deviation as a function of the electrode composition may influence the final electrochemical performance.

On the other hand, non-linear modelling based on artificial neural networks was carried out employing the EIS experimental values corresponding to the electrode polarization resistance at 650 °C and the activation energy for the whole experimental space. This model allows for the identification of compositions minimizing the polarization resistance with low activation energy values. The modelling results are shown in the ternary diagram of Figure 8b-c and these figures allow visualizing clearly the most interesting composition region for both figures of merit, confirming and extending the conclusions extracted previously. In this figure, the calculated values for electrode polarization resistance are displayed in logarithmic scale whilst activation energy is in linear scale. Figure 8b-c reveals that samarium-rich compositions (around 66% molar) combine both high electrode polarization resistance values with low activation energies, similar to those shown by the Sm1SFC sample. On the other hand, lanthanum-praseodymium combinations have lower R_p and similar activation energy values than those coming from the Ln1SFC compositions (Ln = La and Pr), while praseodymium enriched compositions have by far the lowest polarization resistance values at 650 °C. The incorporation of small samarium amounts to the praseodymium-rich lanthanum mixture allows reducing the resistance with a significant decrease in the activation energy and therefore will offer a higher oxygen-reduction activity at lower temperatures.

3.4 Performance of fully-assembled cells SOFC

The electrochemical performance (I-V and power density curves at 600 and 650 °C) corresponding to fully-assembled anode-supported cells with cathodes based on a single-lanthanide Pr1SFC compound and the most promising La_{0.5}Pr_{0.5}SFC compound are displayed in Figure 9. It can be observed that the cell with the La_{0.5}Pr_{0.5}SFC cathode performs significantly better for both tested temperatures and this is ascribed to an improvement in the oxygen reduction processes taking place in the cathode. From the I-V curves, it can be calculated the minimum slope (lowest ASR -area specific resistance-) obtained in the linear ohmic regime. These minimum ASR values are lower

for the La_{0.5}Pr_{0.5}SFC cathode for both temperatures: Pr1SFC = 1.15 Ω·cm² (at 0.49 A·cm⁻², 600 °C) and 0.48 Ω·cm² (at 1.23 A·cm⁻², 650 °C); La_{0.5}Pr_{0.5}SFC = 0.91 Ω·cm² (at 0.67 A·cm⁻², 600 °C) and 0.39 Ω·cm² (at 1.5 A·cm⁻², 650 °C). As a consequence, the maximum power densities obtained for La_{0.5}Pr_{0.5}SFC cathode-based cell are significantly higher than those obtained for the parent Pr1SFC cathode and they are shifted to higher current density values. On the other hand, the observed improvement in the cell performance is not as high as expected from the results obtained through cathode optimization using symmetrical cells. This can be explained considering that other resistances not related to cathode processes are also limiting the cell performance at intermediate temperature. Specifically, resistances related to anode processes and the conduction through the bilayered GDC/8YSZ electrolyte are in the same order of magnitude as the cathode contributions. This situation has been confirmed by EIS analysis of the cells and varying the oxygen and hydrogen concentration in the anode and cathode chambers, respectively (see Supplementary Material, Figure S2). It has been reported [40] that the porous GDC protective layer produced by screen printing and sintered at 1250 °C has a negative effect due to the formation of a GDC-8YSZ solid solution with a reduced ionic conductivity in the interface between both electrolyte layers (See Figure S4 in Supplementary Material).

4 Conclusions

A significant reduction in the electrode polarization resistance is achieved when incorporating simultaneously various lanthanides in the strontium doped ferrite-cobaltite perovskite. The intrinsic properties of each single lanthanide (La, Pr or Sm) compound can be enhanced by combining two or the three lanthanides for operating as electrodes for oxygen activation. Indeed, the (La_{0.5}Pr_{0.5})_{0.58}Sr_{0.4}Fe_{0.8}Co_{0.2}O_{3-δ} composition has the lowest polarization resistance values when analyzed in a symmetrical GDC-based cell at 650 °C. Praseodymium rich (La_{0.17}Pr_{0.66}Sm_{0.17})_{0.58}Sr_{0.4}Fe_{0.8}Co_{0.2}O_{3-δ} ternary composition has also lower polarization resistance values whilst (La_{0.5}Sm_{0.5})_{0.58}Sr_{0.4}Fe_{0.8}Co_{0.2}O_{3-δ} performs better at the lowest measured temperatures. This change in electrode polarization resistance reduction is explained in terms of activation energy. Indeed, single samarium Sm_{0.58}Sr_{0.4}Fe_{0.8}Co_{0.2}O_{3-δ} composition has the lowest activation energy values and when combining samarium with praseodymium or lanthanum in (Ln-Sm)_{0.58}Sr_{0.4}Fe_{0.8}Co_{0.2}O_{3-δ} (Ln = La or Pr) the activation energy is lessened, generating compositions with acceptable polarization resistance at the highest tested temperatures but with promising low polarization resistance values at the lowest measured temperatures. This reduction in electrode polarization resistance would result in higher power density values when the new compositions with lanthanide combinations are applied as SOFC cathodes in the intermediate temperature range. Nevertheless, the whole cell performance is significantly influenced by electrolyte and anode-related resistances, whereas there is still room for improvement of the cathode microstructure.

Acknowledgements

Financial support by the Universitat Politècnica de València (Grant UPV-2007-06), the Spanish Ministry for Science and Innovation (Project ENE2008-06302/CON) and ExxonMobil through the ExxonMobil Chemical European Science and Engineering Award 2005 is kindly acknowledged. The authors thank S. Jiménez for material preparation and S. Escolástico for help in different characterization duties. The support

1
2
3 of Forschungszentrum Jülich (IEF-1) is gratefully acknowledged for providing anode-
4 supported cells.
5
6
7
8
9
10
11
12
13
14
15
16
17
18
19
20
21
22
23
24
25
26
27
28
29
30
31
32
33
34
35
36
37
38
39
40
41
42
43
44
45
46
47
48
49
50
51
52
53
54
55
56
57
58
59
60

For Peer Review

References

- [1] See for instance commercial product at http://www.hexis.com/index_e.htm
- [2] O. Yamamoto, Y. Takeda, R. Kanno, M. Noda, *Solid State Ionics* **1987**, *22*, 241.
- [3] V. Tsipis, V. V. Kharton, *J. Solid State Electrochemn* **2008**, *12*, 1367.
- [4] V. A. C. Haanappel, J. Mertens, D. Rutenbeck, C. Tropartz, W. Herzhof, D. Sebold, F. Tietz, *J. Power Sources* **2005**, *141*, 216
- [5] A. Esquirol, N. P. Brandon, J. A. Kilner, M. Mogensen, *Journal of The Electrochemical Society* **2004**, *151*, A1847.
- [6] A. Mai, V. A. C. Haanappel, S. Uhlenbruck, F. Tietz, D. Stöver, *Solid State Ionics* **2005**, *176*, 1341.
- [7] J. M. Serra, H.-P. Buchkremer, *Journal of Power Sources* **2007**, *172*, 768.
- [8] C. Xia, W. Rauch, F. Chen, M. Liu, *Solid State Ionics* **2002**, 149, 11.
- [9] M. B. Phillipps, N. M. Sammes, O. Yamamoto, *Solid State Ionics* **1999**, *123*, 131
- [10] J. Piao, K. Sun, N. Zhang, X. Chen, S. Xu, D. Zhou, *Journal of Power Sources* **2007**, *172*, 633.
- [11] V. N. Tikhonovich, V. V. Kharton, E. N. Naumovich, A. A. Savitsky, *Solid State Ionics* **1998**, *106*, 197.
- [12] J. M. Serra, V. B. Vert, M. Betz, V. A. C. Haanappel, W. A. Meulenberg, F. Tietz, *Journal of The Electrochemical Society* **2008**, *155*, B207
- [13] J. Peña-Martínez, D. Marrero-López, D. Pérez-Coll, J.C. Ruiz-Morales, P. Núñez, *Electrochimica Acta* **2007**, *52*, 2950.
- [14] L. M. Rodriguez-Martinez, K. Vidal, L. Ortega-San-Martin, M. L. Nó, T. Rojo, A. Laresgoiti, M. I. Arriortua, “The Effect of A-Site Parameters in the Properties of AFeO_{3-δ} Perovskites” in *Proceedings of the European Fuel Forum* **2008**, A0604, Lucerne, Switzerland

- 1
2
3
4 [15] Z. Shao, S. M. Haile, *Nature* **2004**, *431*, 170
5
6 [16] M. Pechini, *U.S. Pat. 3,330,697* 1967
7
8 [17] W. G. Wang, M. Mogensen, *Solid State Ionics* **2005**, *176*, 457
9
10 [18] K. Kammer; *Solid State Ionics* **2006**, *177*, 1047
11
12 [19] S. Asthana, J. Dho, D. Bahadur, *Solid State Communications* **2007**, *143*, 522
13
14 [20] R. D. Shannon, *Acta Crystallographica Section A* **1987**, *32*, 751.
15
16 [21] Y. Q. Jia, *Journal of Solid State Chemistry* **1991**, *95*, 184
17
18 [22] X'Pert HighScore Plus software v. 2.2b, *PANalytical B. V., Almelo, the*
19
20 *Netherlands, 2006*
21
22 [23] N. Dasgupta, R. Krishnamoorthy, K. Thomas Jacob, *Materials Science and*
23
24 *Engineering* **2002**, *B90*, 278.
25
26 [24] L.-W. Tai, M. M. Nasrallah, H. U. Anderson, D. M. Sparlin, S. R. Sehlin, *Solid*
27
28 *State Ionics* **1995**, *76*, 273
29
30 [25] M. A. Alario-Franco, R. Ruiz-Bustos, A. J. Dos Santos-García, *Inorganic*
31
32 *Chemistry* **2008**, *47*, 6475.
33
34 [26] V. B. Vert, J. M. Serra, *Fuel Cells* **2009**, *5*, 663.
35
36 [27] J. W. Erning, T. Hauber, U. Stimming, K. Wippermann, *Journal of Power Sources*
37
38 **1996**, *31*, 205.
39
40 [28] S. B. Adler, *Chemical Review* **2004**, *104*, 4791.
41
42 [29] K. Masuda, A. Kaimai, K. Kawamura, Y. Nigara, T. Kawada, J. Mizusaki, H.
43
44 Yugami, H. Arashi, *Proceedings of the Fifth International Symposium on Solid Oxide*
45
46 *Fuel Cells (SOFC-V)* **1997**, *97*, 473.
47
48 [30] E. Ivers-Tiffée, A. Weber, H. Schichlein, *Handbook of Fuel Cells Volume 2*, John
49
50 Wiley & Sons Ltd., Chichester, England, **2003**.
51
52 [31] M. Martin, *Diffusion Fundamentals* **2007**, *6*, 39.
53
54
55
56
57
58
59
60

- 1
2
3
4 [32] V. B. Vert, J. M. Serra, "Influence of barium incorporation on the electrochemical
5 performance of $\text{Ln}_{0.58}\text{Sr}_{0.4}\text{Fe}_{0.8}\text{Co}_{0.2}\text{O}_{3-\delta}$ (Ln=La, Pr, Sm) perovskites for oxygen
6 activation at intermediate temperatures" *Fuel Cells* **2009** in press
7
8
9
10
11 [33] R. Baker, J. Guindet, M. Kleitz, *Journal of The Electrochemical Society* **1997**, *144*,
12 2427.
13
14
15
16 [34] S. B. Adler, J. A. Lane, B. C. H. Steele, *Journal of The Electrochemical Society*
17 **1996**, *143*, 3554.
18
19
20
21 [35] B. A. Boukamp, H. J. M. Bowmeester, *Solid State Ionics* **2003**, *157*, 29.
22
23 [36] V. Dusastre, J.A. Kilner, *Solid State Ionics* **1999**, *126*, 163.
24
25
26 [37] N. Trofimenko, H. Ullman, *Solid Sate Ionics* **1999**, *118*, 215
27
28 [38] R. L Cook, A. F. Sammels, *Solid State Ionics* **1991**, *45*, 311
29
30 [39] B. A. Boukamp, M. Verbraeken, D. H. A. Blank, P. Holtappels, *Solid State Ionics*
31 **2006**, *177*, 2539.
32
33
34 [40] N. Jordan, W. Assenmacher, S. Uhlenbruck, V. A. C. Haanappel, H.P.
35 Buchkremer, D. Stöver, W. Mader, *Solid State Ionics* **2008**, *179*, 919
36
37
38
39
40
41
42
43
44
45
46
47
48
49
50
51
52
53
54
55
56
57
58
59
60

Figures Caption

Figure 1. Ternary experimental mixture design of the synthesized perovskite electrode compositions. (See nomenclature key in Table 1)

Figure 2. Room temperature XRD patterns of the synthesized compositions: (a) La1SFC, (b) La0.5Pr0.5SFC, (c) Pr1SFC, (d) La0.5Sm0.5SFC, (e) Sm1SFC, (f) Pr0.5Sm0.5SFC, (g) La0.33Pr0.33Sm0.33SFC, (h) La0.66Pr0.17Sm0.17SFC, (i) La0.17Pr0.66Sm0.17SFC and (j) La0.17Pr0.17Sm0.66SFC. Closed circles correspond to orthorhombic symmetry peaks and plus symbol to minor impurities assigned to CoFe₂O₄ spinel.

Figure 3. Pseudo-cubic (*a'*) lattice parameter computed from the XRD patterns for the different compounds grouped in single, binary and ternary lanthanide-based compositions. Filled bars illustrate the relative proportion amongst the different lanthanides for each cathode compound.

Figure 4. SEM analysis of fracture cross-section of the symmetrical cells after electrochemical testing. Micrographs of graphite sputtered multi-lanthanide electrodes after calcination at 1060 °C supported on the GDC electrolyte. Electrode composition is shown on each picture.

Figure 5. Arrhenius plot of electrode polarization resistance values of all synthesized compositions in the measured temperature range 450-650 °C. *R_p* values have been calculated after fitting the equivalent circuit using the symmetrical cells EIS data. (a) single, (b) binary and (c) ternary compositions data.

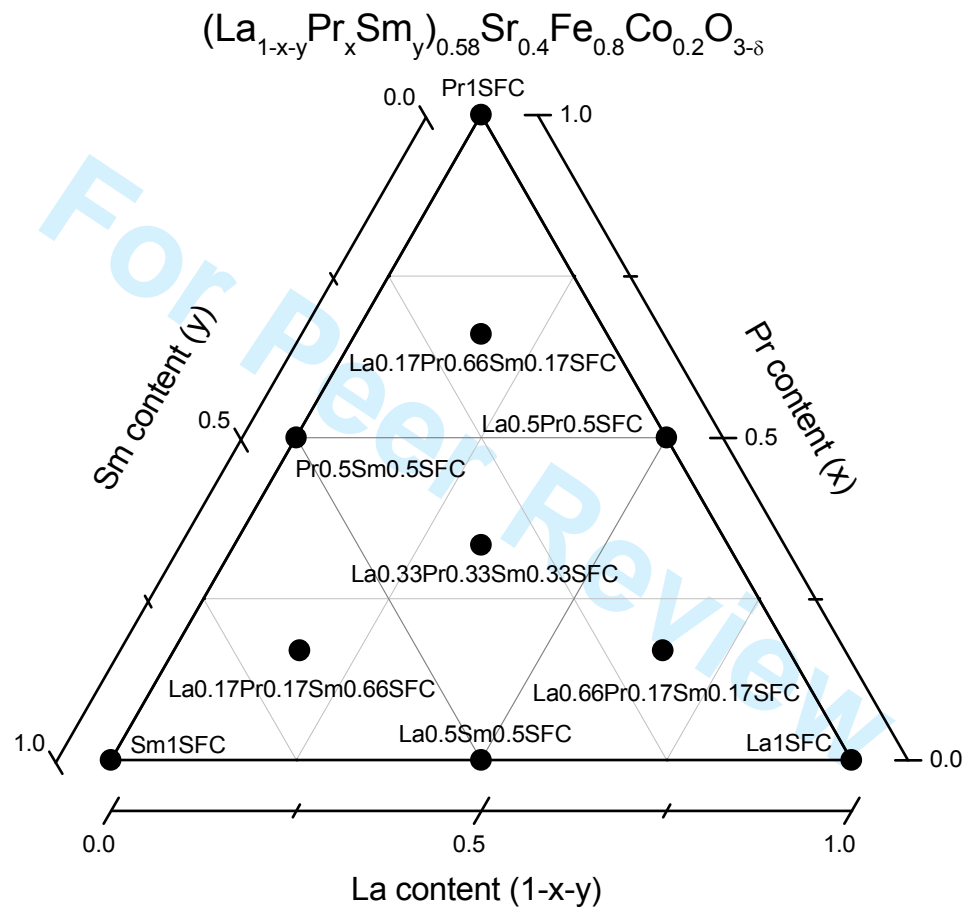
Figure 6. Apparent *R_p* activation energy values (bars) calculated for all measured symmetrical electrode compositions and the corresponding samarium content in % molar (squared line – right-handed axis).

Figure 7. Evolution of polarization resistance and reaction rate constant *k* as a function of operating temperature and oxygen partial pressure for selected electrode compositions. Data points correspond to different oxygen partial pressures: 0.21 atm (solid square); 0.105 atm (open square); and 0.021 atm (cross).

Figure 8. Modelling surface computed for ternary experimental design: (a) simulated values for the pseudo-cubic *a'* cell parameter; (b) simulated values for electrode polarization resistance; and (c) the corresponding activation energy. Contour mappings show the different levels of each magnitude in the 2D space of the mixture design. The number of levels has been fixed to a reduced number for clarity.

Figure 9. Voltamperometry and power density values obtained for anode-supported fuel cells based on NiO-8YSZ/8YSZ/GDC anode/electrolyte/protective layer system with Pr1SFC (diamonds) and La0.5Pr0.5SFC (squares) cathodes at 600 and 650 °C.

Figure 1



1
2
3
4
5
6
7
8
9
10
11
12
13
14
15
16
17
18
19
20
21
22
23
24
25
26
27
28
29
30
31
32
33
34
35
36
37
38
39
40
41
42
43
44
45
46
47

Figure 2

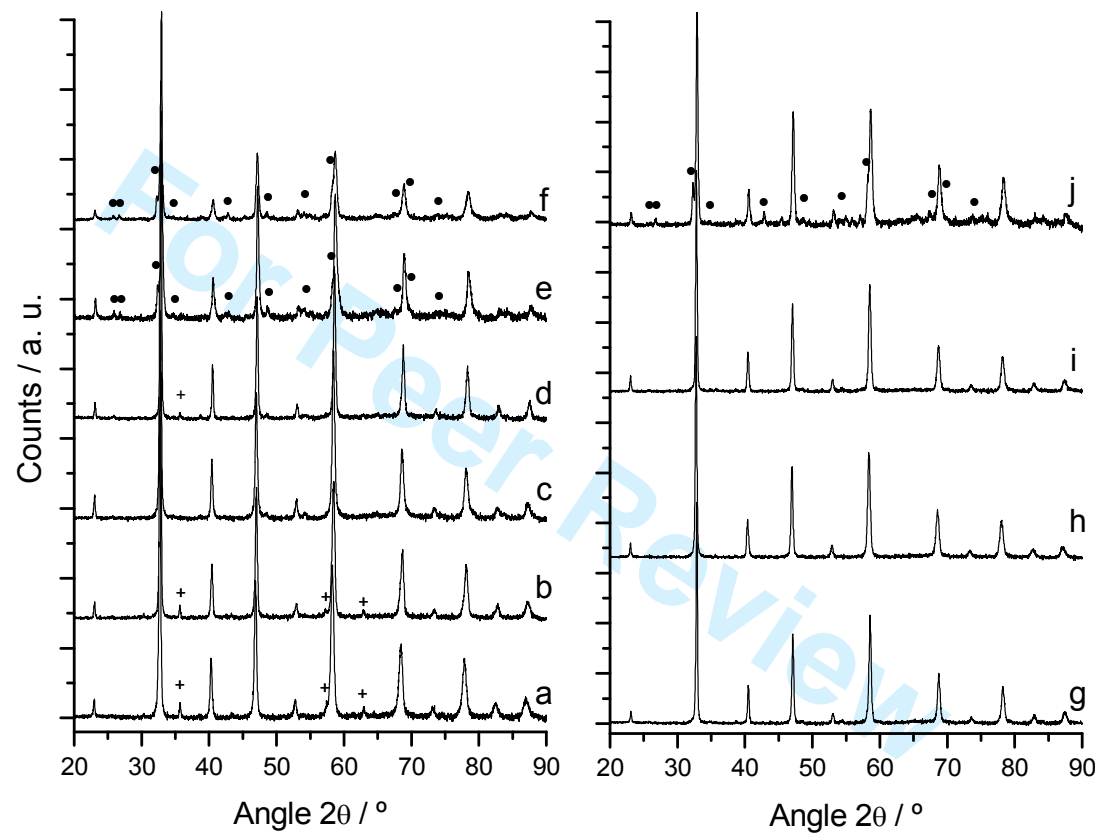


Figure 3

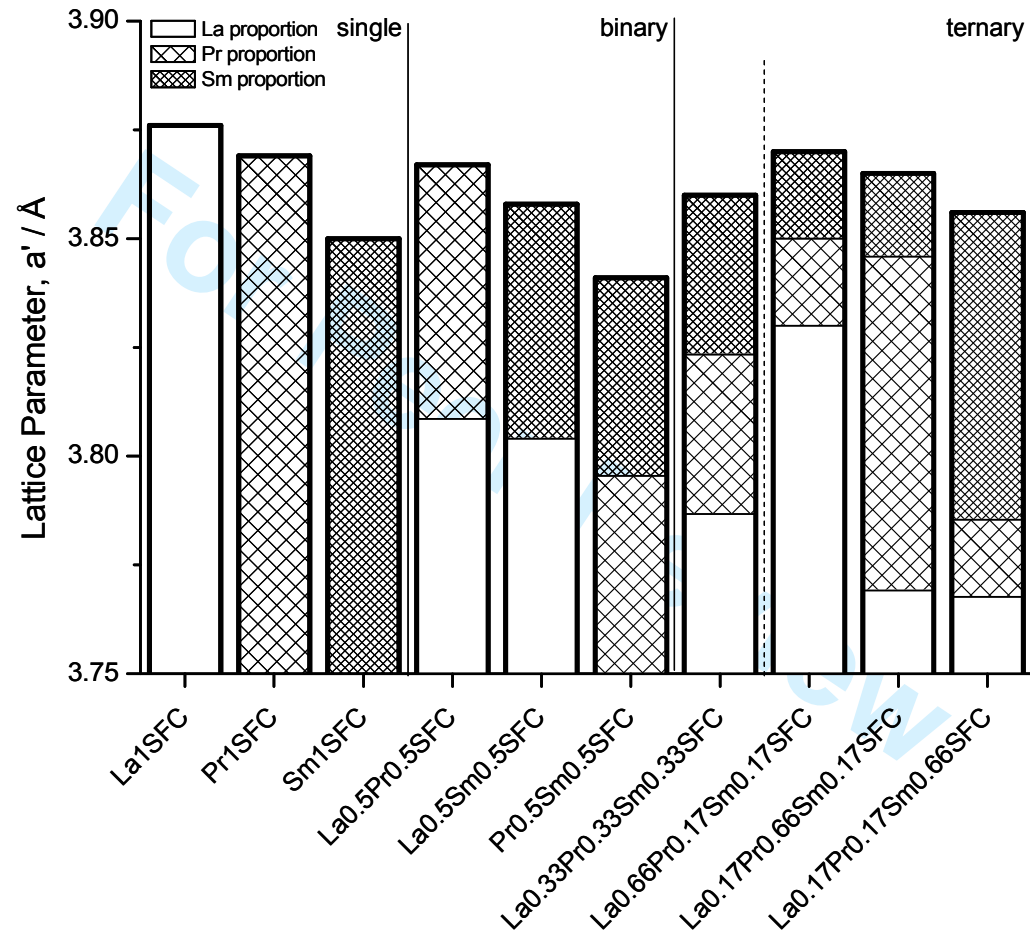


Figure 4

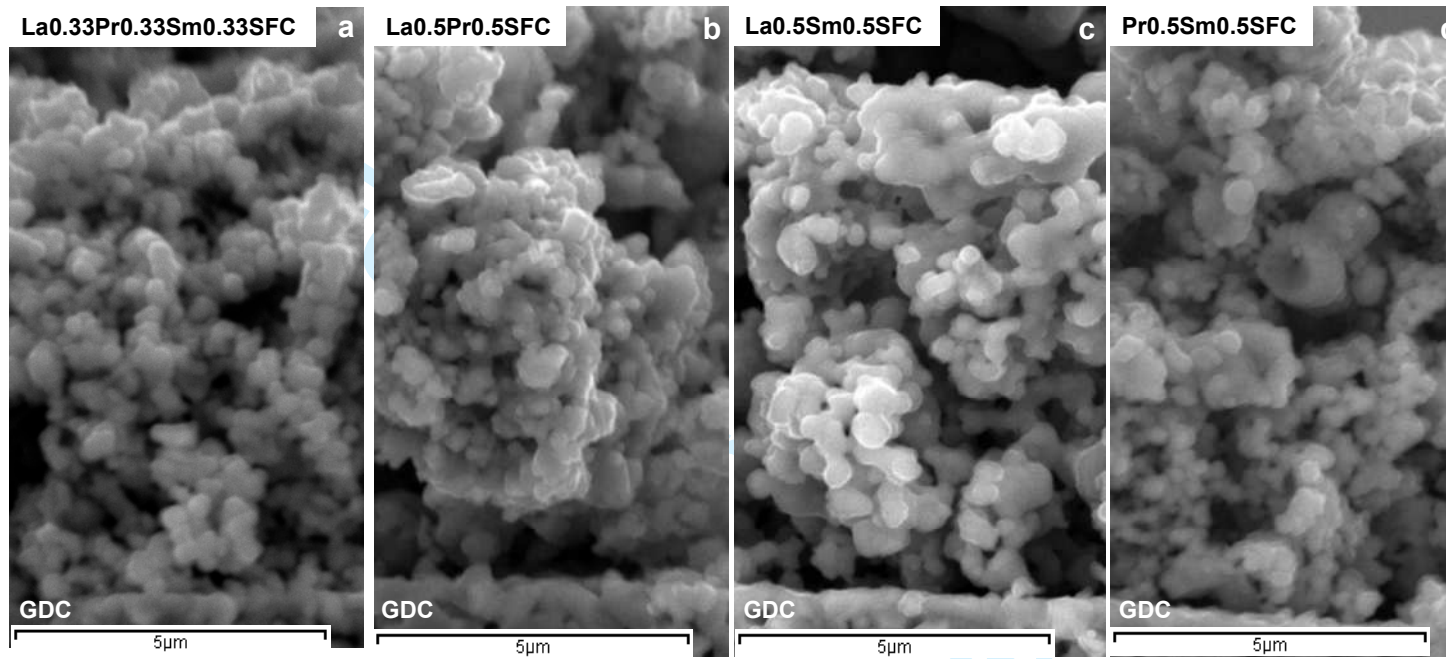


Figure 5

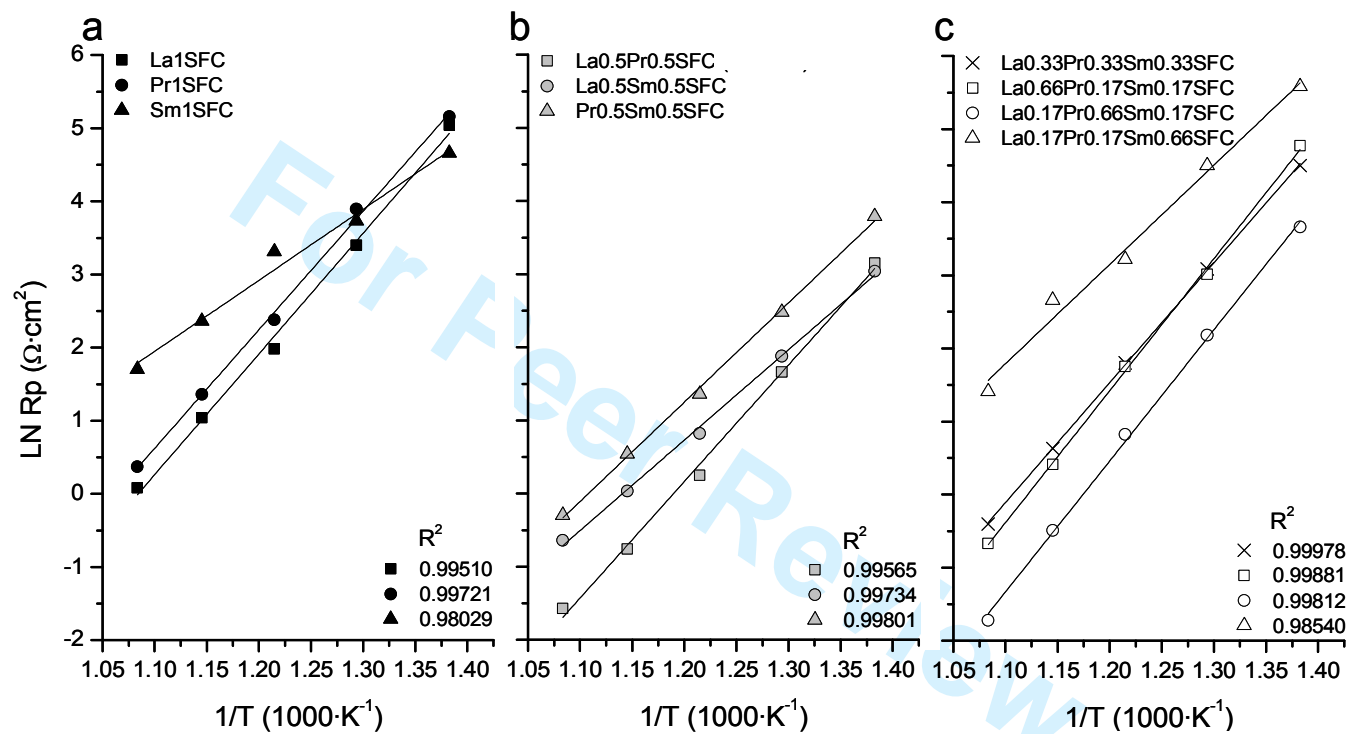


Figure 6

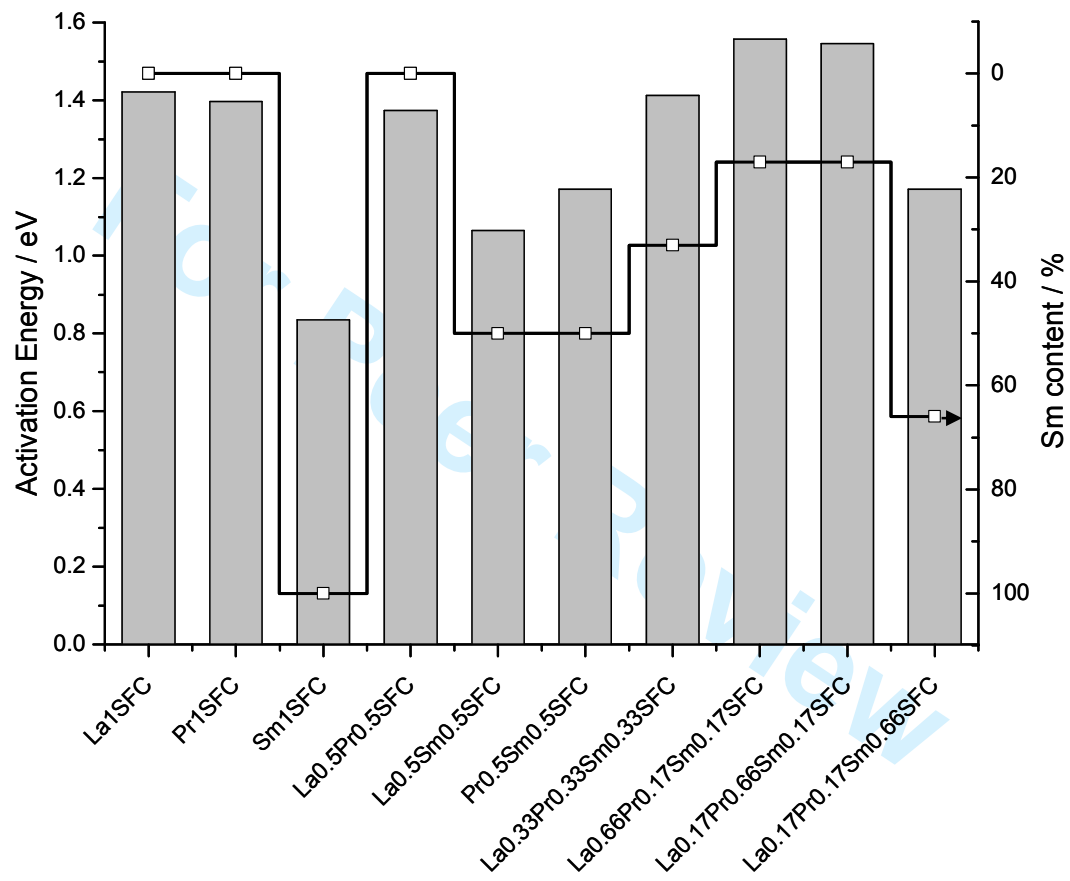


Figure 7

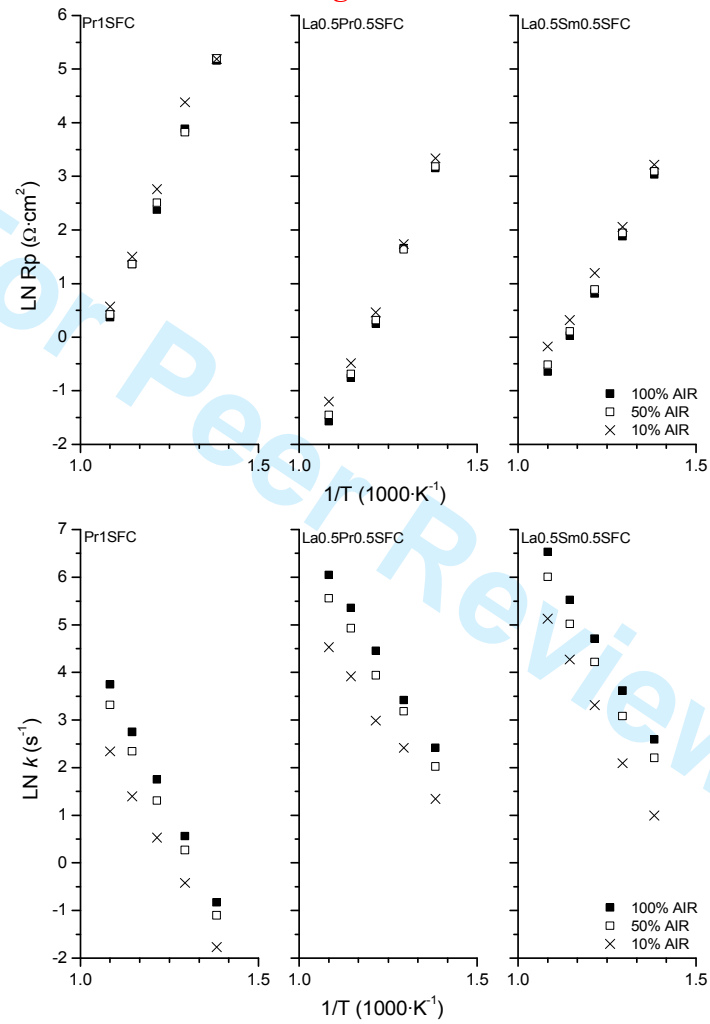


Figure 8

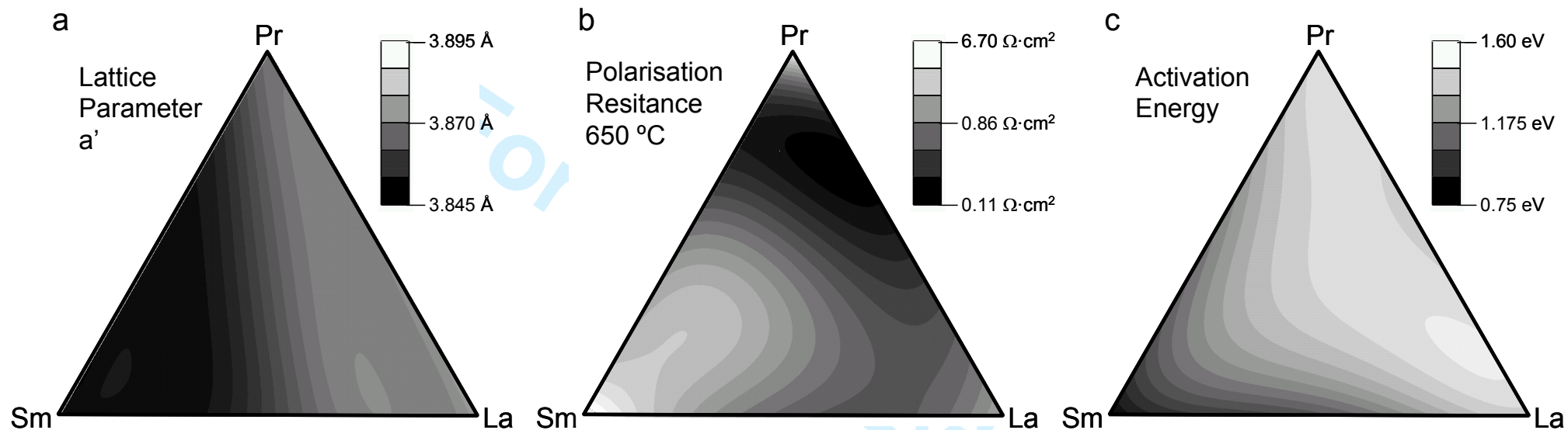
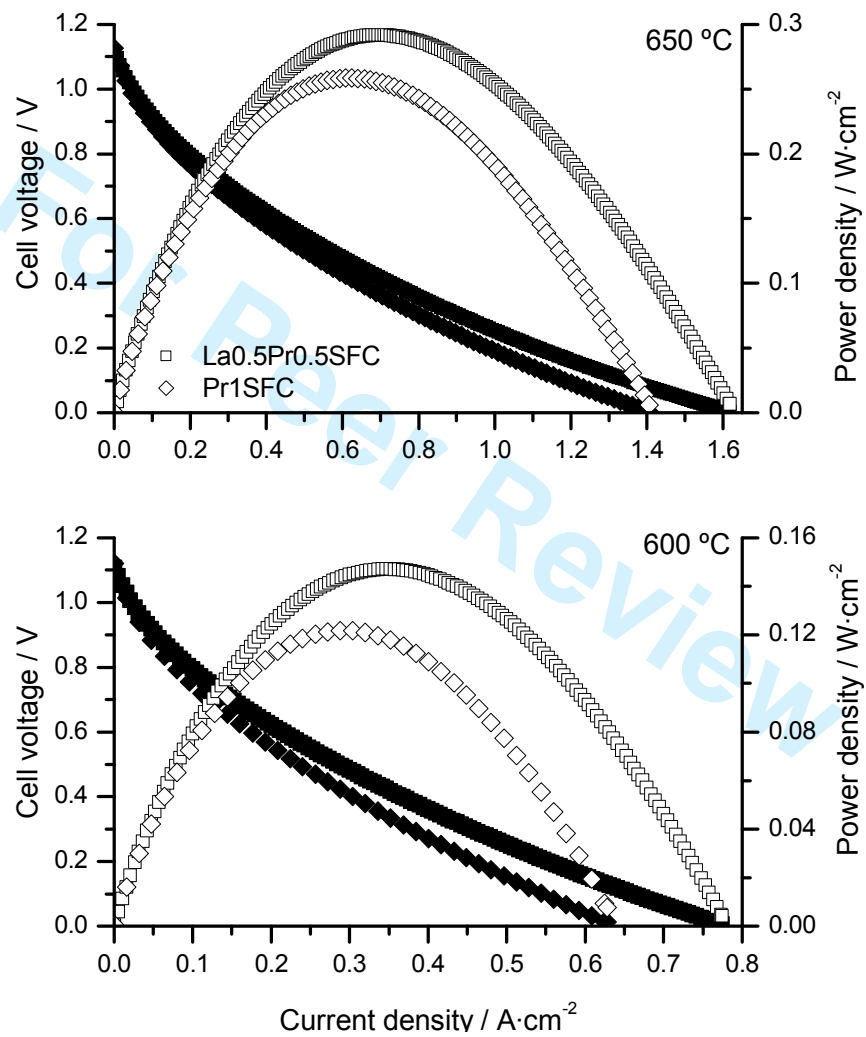


Figure 9



1
2
3
4
5
6
7
8
9
10
11
12
13
14
15
16
17
18
19
20
21
22
23
24
25
26
27
28
29
30
31
32
33
34
35
36
37
38
39
40
41
42
43
44
45
46
47

Composition name	L	P	S	Stoichiometry
La1SFC	1	0	0	$\text{La}_{0.58}\text{Sr}_{0.4}\text{Fe}_{0.8}\text{Co}_{0.2}\text{O}_{3-\delta}$
Pr1SFC	0	1	0	$\text{Pr}_{0.58}\text{Sr}_{0.4}\text{Fe}_{0.8}\text{Co}_{0.2}\text{O}_{3-\delta}$
Sm1SFC	0	0	1	$\text{Sm}_{0.58}\text{Sr}_{0.4}\text{Fe}_{0.8}\text{Co}_{0.2}\text{O}_{3-\delta}$
La0.5Pr0.5SFC	0.5	0.5	0	$\text{La}_{0.29}\text{Pr}_{0.29}\text{Sr}_{0.4}\text{Fe}_{0.8}\text{Co}_{0.2}\text{O}_{3-\delta}$
La0.5Sm0.5SFC	0.5	0	0.5	$\text{La}_{0.29}\text{Sm}_{0.29}\text{Sr}_{0.4}\text{Fe}_{0.8}\text{Co}_{0.2}\text{O}_{3-\delta}$
Pr0.5Sm0.5SFC	0	0.5	0.5	$\text{Pr}_{0.29}\text{Sm}_{0.29}\text{Sr}_{0.4}\text{Fe}_{0.8}\text{Co}_{0.2}\text{O}_{3-\delta}$
La0.33Pr0.33Sm0.33SFC	0.33	0.33	0.33	$\text{La}_{0.1914}\text{Pr}_{0.1914}\text{Sm}_{0.1914}\text{Sr}_{0.4}\text{Fe}_{0.8}\text{Co}_{0.2}\text{O}_{3-\delta}$
La0.66Pr0.17Sm0.17SFC	0.66	0.17	0.17	$\text{La}_{0.3828}\text{Pr}_{0.0986}\text{Sm}_{0.0986}\text{Sr}_{0.4}\text{Fe}_{0.8}\text{Co}_{0.2}\text{O}_{3-\delta}$
La0.17Pr0.66Sm0.17SFC	0.17	0.66	0.17	$\text{La}_{0.0986}\text{Pr}_{0.3828}\text{Sm}_{0.0986}\text{Sr}_{0.4}\text{Fe}_{0.8}\text{Co}_{0.2}\text{O}_{3-\delta}$
La0.17Pr0.17Sm0.66SFC	0.17	0.17	0.66	$\text{La}_{0.0986}\text{Pr}_{0.0986}\text{Sm}_{0.3828}\text{Sr}_{0.4}\text{Fe}_{0.8}\text{Co}_{0.2}\text{O}_{3-\delta}$

Table 1: Synthesized cathode compositions, where L, P and S values correspond to the stoichiometric numbers of $(\text{La}_L\text{Pr}_P\text{Sm}_S)_{0.58}\text{Sr}_{0.4}\text{Fe}_{0.8}\text{Co}_{0.2}\text{O}_3$ perovskite formula. Last column shows the final stoichiometry of each composition.